# Drexel University

# Annual Progress Report: 2011 Formula Grant

**Reporting Period**

July 1, 2013 – June 30, 2014

**Formula Grant Overview**

Drexel University received $1,320,271 in formula funds for the grant award period January 1, 2012 through December 31, 2014. Accomplishments for the reporting period are described below.

**Research Project 1: Project Title and Purpose**

*An Interdisciplinary Approach to Directly Identify Changes in the miRNA-targeted mRNA Population Induced by HBV Infection* – This project will identify specific changes in the population of RISC-associated micro(mi)RNAs and their targeted mRNAs in HBV-infected hepatocytes. Further, bioinformatic analyses and data-mining will be used to define signaling networks that are affected by these alterations in miRNA targeting. We will use these results to propose mechanistic studies to determine how HBV controls miRNA signaling networks in ways that promote HBV replication and sensitize hepatocytes to the continued inflammatory insults associated with chronic HBV infection, ultimately leading to liver cancer. An understanding of these regulatory networks will help to identify new points of intervention in the treatment of HBV-induced progressive liver disease.

**Anticipated Duration of Project**

1/1/2012 – 12/31/2014

**Project Overview**

This project will define how alterations in the expression of specific microRNAs (miRNAs) that are induced by infection of primary human hepatocytes (PHHs) with hepatitis B virus (HBV) can lead to changes in cell physiology that promote viral replication and deregulation of pathways that control cell proliferation. miRNAs are known to be key players with a role in pathways that govern fundamental cell processes such as proliferation, differentiation, apoptosis, and response to stress. Changes in miRNA expression have been reported in hepatocytes upon infection with HBV or overexpression of HBV X protein (HBx). Despite the identification of some miRNA-targeted mRNAs, there is no comprehensive understanding of the mRNAs that are regulated by this process in infected cells.

We hypothesize that HBV infection changes the population of miRNA-targeted mRNAs to alter normal hepatocyte physiology and create an environment that favors HBV replication and

contributes to hepatocellular carcinoma (HCC) development. To test our hypothesis we will address the following aims:

Aim 1: Establish photoactivatable ribonucleoside-enhanced crosslinking and immunoprecipitation (PAR-CLIP) technology and data analysis parameters for direct identification of RISC-associated miRNAs and targeted mRNAs in cultured PHHs.
Aim 2: Characterize changes in the miRNA population and miRNA-targeted mRNAs induced by HBV infection of PHHs.
Aim 3: Determine the impact of miRNA targeting of specific mRNAs identified in Aim 2 on HBV replication and hepatocyte physiology. We will use a new technology, PAR-CLIP to directly identify and quantify the mRNAs that are targeted by RISC-associated miRNAs in HBV-infected PHHs.

Bioinformatic analyses of our results and data mining of open access gene expression data will be combined to develop a signaling-system interaction network and a set of interlinked signaling modules to predict pathways that are affected by HBV infection and drive HCC development. The role of miRNAs that are predicted to occupy key nodal points in the interaction map will be experimentally validated by altering their expression level, using miRNA mimics or inhibitors in PHHs, and characterizing the effects on HBV replication and hepatocyte physiology.

**Principal Investigator**

Michael J. Bouchard, PhD
Associate Professor
Drexel University
245 North 15th St., MS 497
New College Building, Rm 11312
Philadelphia, PA 19102

**Other Participating Researchers**

Laura F. Steel, PhD; Aydin Tozeren, PhD – employed by Drexel University

**Expected Research Outcomes and Benefits**

This project will help us to understand the mechanisms by which HBV infection alters miRNA expression patterns, the cell signaling pathways that they mediate, and the extent to which these alterations benefit the virus or promote disease progression. Although chronic HBV infection is recognized as a major risk factor for liver disease, including fibrosis, cirrhosis, and hepatocellular carcinoma (HCC), the cellular mechanisms that underlie disease progression are incompletely understood. Studies of changes in miRNA expression have been informative, particularly in providing biomarkers for the later stages of liver disease and HCC. However, liver disease progresses over decades and is often only detected at late stages when treatment options are limited or ineffective. We expect that our studies will provide new information on how cellular signaling networks are disrupted at early stages of viral infection in ways that alter the cellular response to continuing inflammatory insults, thereby setting the stage for the

development of liver disease. By identifying the mRNA targets of specific miRNAs whose expression or function is altered by viral infection, we will uncover potential therapeutic targets and opportunities for earlier and more effective therapeutic intervention in the devastating liver diseases caused by chronic HBV infection. By increasing our understanding of the cellular pathways that are deregulated in infected hepatocytes, our studies may also point to common therapeutic targets for other causes of HCC.

**Summary of Research Completed**

Progress on Aim 1

During this funding period, we continued to optimize conditions for conducting PAR-CLIP in primary hepatocytes. However, due to technical issues with this procedure, we changed to a similar procedure, high-throughput sequencing of RNA isolated by crosslinking immunoprecipitation (HITS-CLIP), and continued studies in cultured primary hepatocytes. The only difference between the HITS-CLIP protocol and the PAR-CLIP protocol is the omission of 4-SU for labeling and the direct crosslinking of all mRNAs and miRNAs to the RNA-induced silencing complex (RISC). Due to personnel changes in the facility of our primary human hepatocyte supplier, this service was unavailable for 8 months, and we therefore proceeded with optimizing conditions for these studies in cultured primary rat hepatocytes (protocol #20057, approved by Drexel University IACUC). An outline of the procedure for HITS-CLIP and PAR-CLIP (note the similarity in these procedures) is shown in Figure 1.

HITS-CLIP, similar to PAR-CLIP, is very technically challenging, and each and every step of the protocol (Fig. 1) has required extensive modifications and optimization, which has consumed this entire remaining year of funding. We were initially able to confirm that we could immunoprecipitate and detect Ago, a component of RISC in cultured primary rat hepatocytes. We then spent a considerable amount of time and effort in optimizing crosslinking of RNA to RISC, labeling the RNA, and then immunoprecipitating the crosslinked complex (Figures 1 and 2, right panels). After encountering numerous technical barriers, we contacted, consulted, and received advice from two research groups that had initially reported results using these types of assays (Tuschl's group at Rockefeller University and the Kaestner research group at the University of Pennsylvania). It became apparent that all previous uses of this procedure had been conducted in cell lines and with immunoprecipitation of Ago that was expressed from a transfected vector (i.e., previous studies from these groups did not use primary cells or immunoprecipitation of endogenous Ago). This suggested that the procedure might not be possible in cultured primary hepatocytes; however, we proceeded with additional attempts at optimization. After about 6 months of trial-and-error, we concluded that the inconsistency of results using this protocol and the low level of Ago in cultured primary hepatocytes precluded a reasonable use of this system in primary hepatocytes (Figure 2, right panel, red box shows the extremely low levels of immunoprecipitated, crosslinked RNA that was acquired from primary rat hepatocytes.

We next changed our cell model to the next best available liver model system, AML12 cells. This immortalized mouse hepatocyte cell line was derived from a TGF-alpha transgenic mouse and is considered as close to normal hepatocytes as possible for a cell line (i.e., these cells express many markers of fully differentiated hepatocytes and have been used for studies of "normal" hepatocyte physiology). We repeated optimization of the HITS-CLIP procedure in

these cells, which again required extensive trial and error. However, when HITS-CLIP was performed with cultured AML12 cells, the results of these studies suggested that considerably higher levels of crosslinked mRNA and miRNAs can be acquired as compared to cultured primary hepatocytes (Figure 2). This promising result led us to further optimize the system by determining the optimal number of cells and conditions for crosslinking of RNA and immunoprecipitation of RISC (Figure 3). Further analysis has suggested that we had finally isolated crosslinked RNA; however, additional tests confirmed that this RNA was unlikely to be crosslinked mRNA and demonstrated that immunoprecipitation of RISC complexes with antibodies targeting endogenous Ago generates highly inconsistent results. Our recent discussions at conferences with others who have attempted this procedure supports our conclusion that the HITS-CLIP (and PAR-CLIP) procedures work best in established cell lines and with over-expression of Ago from a transfected vector. As this is counter to our original goal, which was to identify endogenous changes in the miRNA and mRNA RISC profiles in HBV-infected hepatocytes, we used the remaining funds to perform a transcriptome mRNA sequence study in HBV-infected primary rat hepatocytes and also analyze expression of miRNAs in the same cells. We believe that this will provide us with the next best analysis of miRNA and mRNA profiles in the same cells. We are currently awaiting the results of these sequencing studies.

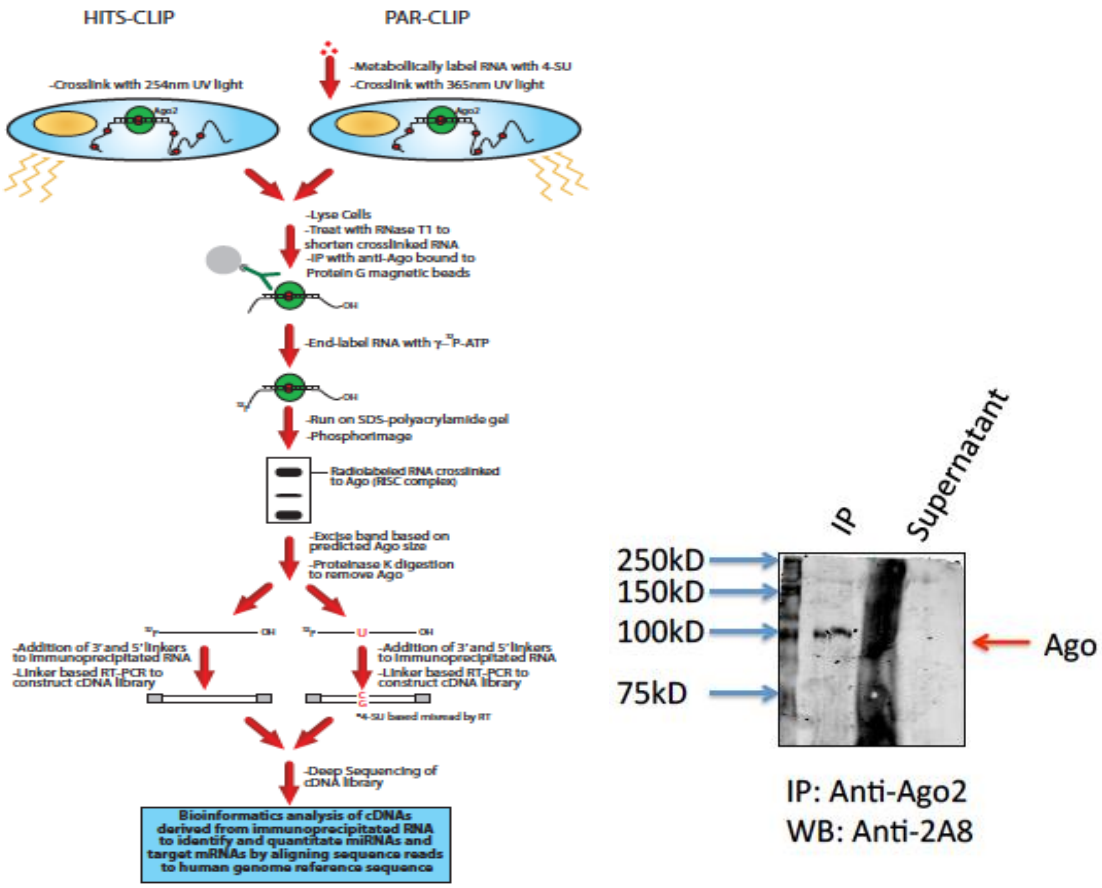


Figure 1: Left panel shows the step-by-step outline of the HITS-CLIP and PAR- CLIP procedures. Right panel shows successful immunoprecipitation of Ago from cultured primary rat hepatocytes.

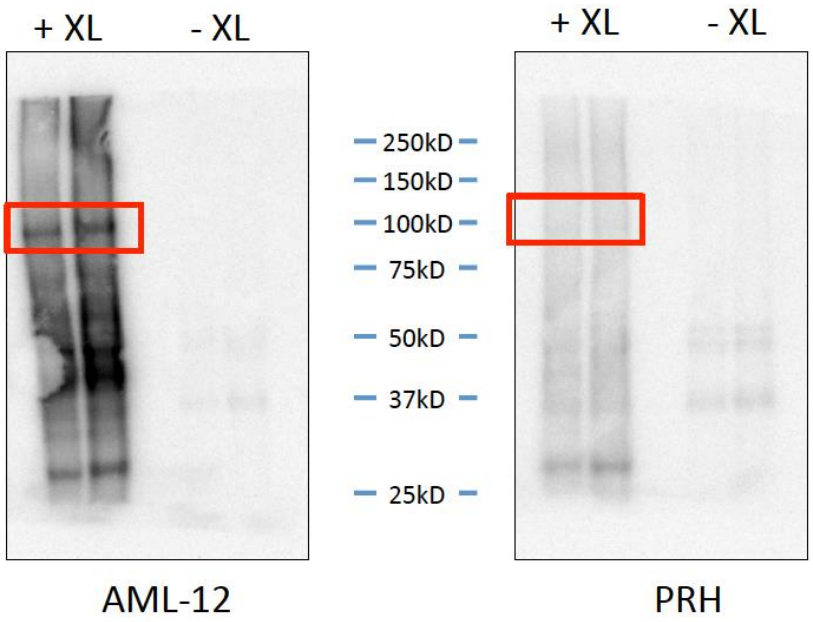


Figure 2: Right panel shows successful crosslinking of RNA to immunoprecipitated RISC; Left panel serves as a comparison in cultured primary rat hepatocytes. Although longer exposure showed immunoprecipitated, crosslinked RNA, the efficiency of this reaction is such that the enormous amounts of hepatocytes that would be required precludes use of this procedure.

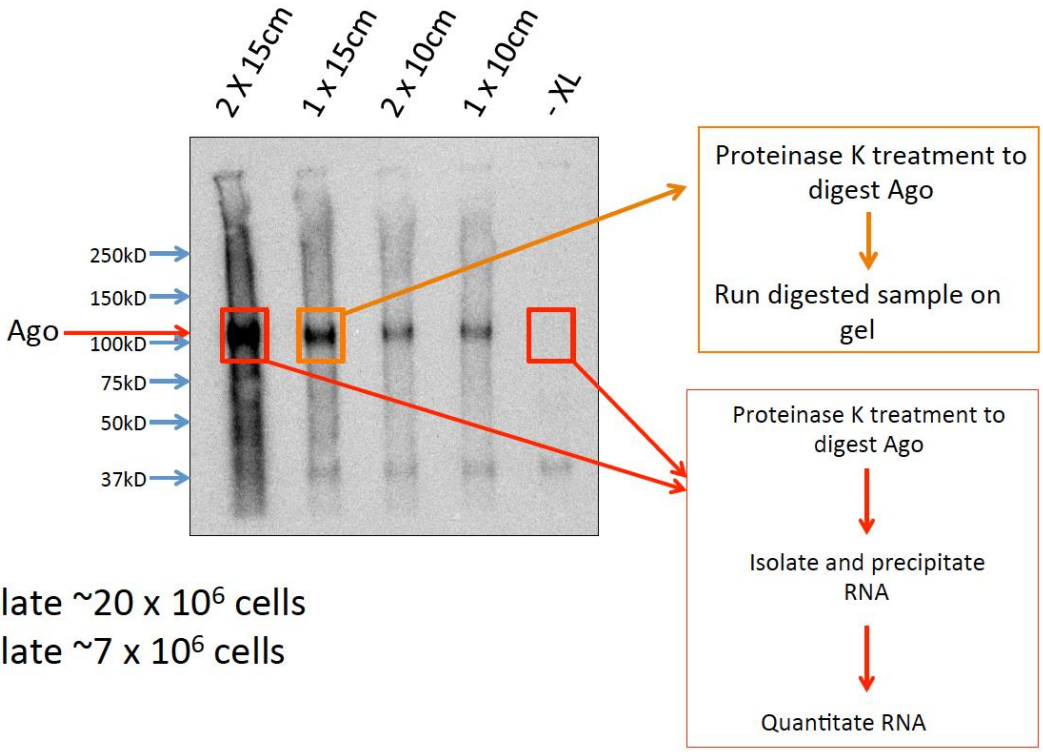


Figure 3: Immunoprecipitated Ago complexes with crosslinked RNA in various numbers of cells. Right panel shows procedure used to eventually isolate and quantify RNA.

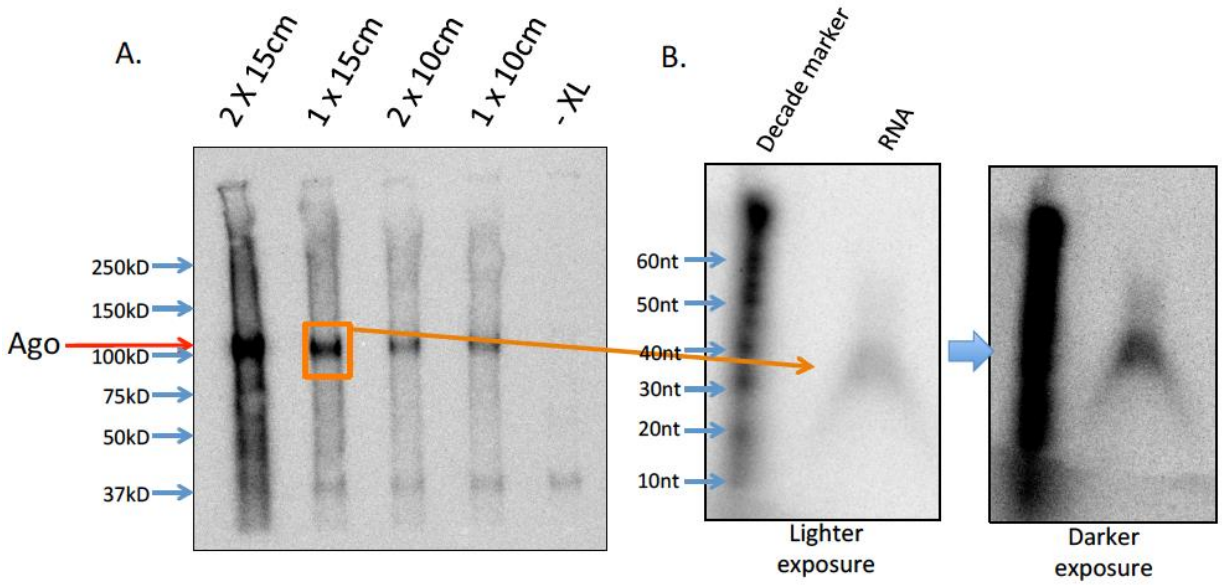


Figure 4: Left panel is same as left panel in Figure 3. Left panels show purified RNA run on an acrylamide gel. See text for discussion.

## Research Project 2: Project Title and Purpose

*Novel Anti-Pancreatic Cancer Peptides from the ras-p21 Protein* – We will establish that a kinase super-complex with oncogenic k-ras forms in pancreatic cancer, but not in normally proliferating cells, that is disrupted by peptides synthesized from oncogenic ras-p21 containing oncogenic amino acid substitutions that induce stereotypical changes in the three-dimensional structures of six domains of the oncogenic proteins. Two such peptides corresponding to these domains, PNC-2 and PNC-7, will then be tested to selectively arrest pancreatic cancer cell growth. We will test PNC-2 and PNC-7 for their ability to eradicate human pancreatic cancers transplanted into nude mice. We will also test the ability of these peptides to eradicate a syngeneic pancreatic cancer utilizing an established murine model.

### Anticipated Duration of Project

1/1/2012 – 12/31/2014

### Project Overview

Most pancreatic cancers are caused by a mutant, oncogenic protein called ras-p21. This protein, but not its normal form, causes normal human cells to transform into malignant ones and causes egg cells (oocytes) to divide. We have found in oocytes that the mutant protein causes cell division in an uncontrolled manner by forming large super-complexes with other proteins that stimulate cell division and maintains them in the complex so that they continuously tell the cell to divide. In this project, we will lyse human pancreatic cells and immunoprecipitate (IP) k-ras from the lysates using a k-ras-specific monoclonal antibody and blot the IPs for each of the component proteins (ras, raf, MEK, MAPK, JNK) with the appropriate antibody. Detection will be accomplished using anti-mouse secondary antibody with an ECL chemiluminescence detection kit.

We will further blot the IPs for the phosphorylated forms of each of these kinases in the super-complex using phospho-protein-specific antibodies. Since we have developed an untransformed pancreatic acinar cell line (BMRPA1) in our laboratory, we will perform the same studies on lysates from these cells as controls to demonstrate that no such complex forms in these cells. TUC-3 cells are ras transformed rodent BMRPA1 cells.

Secondly, we have developed two new peptides, called PNC-2 and PNC-7 that are from parts of ras-p21 that block cell division caused by the mutant ras-p21 protein but have no effect on the normal form of this protein, as previously shown in our oocyte model. We will test the effect of these peptides on complex formation and alternate pathway activation in pancreatic cancer cell lines. Treated cells will be lysed and the lysates subjected to the above protocols to determine the level of each protein in the complex and alternate pathway activation. Moreover, we will also test whether these peptides break up the large complexes with mutant ras-p21. We will also test another peptide GST 35-50 that blocks the activation of one of the important targets of mutant ras-p21, called JNK, which likewise selectively blocks oncogenic, mutant ras-p21 in oocytes. Lastly, we will test these peptides on pancreatic cancers that grow in animal models, i.e., nude mice and syngeneic mouse models that have pancreatic cancer.

*Specific Aims.*
1. We will establish that a kinase super-complex with oncogenic k-ras forms in pancreatic cancer, but not in normally proliferating cells, that is disrupted by PNC-2 and PNC-7 explaining why these peptides could selectively arrest pancreatic cancer cell growth.
2. We will then test PNC-2 and PNC-7 for their ability to eradicate pancreatic cancers transplanted into nude mice. We will also test these peptides for their ability to eradicate a syngeneic pancreatic cancer utilizing an established murine model.

**Principal Investigator**

Wilbur Bowne, MD
Associate Professor of Surgery/ Cellular and Molecular Biology
Drexel University College of Medicine
Department of Surgery
245 N. 15th Street
Philadelphia, PA 19102

**Other Participating Researchers**

Jane Clifford, PhD; Kim Wasko, CVT,VTS; Katlin Davitt – employed by Drexel University College of Medicine
Matthew R. Pincus, MD, PhD – employed by SUNY-Brooklyn
Victor Adler, MD, PhD – consultant

**Expected Research Outcomes and Benefits**

We anticipate that selected pancreatic cancer cells will have super-complexes of the activated kinases with k-ras. Since we have developed and obtained untransformed pancreatic cell lines

(BMRPA1) in our laboratory, we will perform the same studies on lysates from these cells during growth as controls to demonstrate that no such complex forms in these cells. In cells treated with PNC 2 and PNC-7, we expect that the supercomplex levels will be reduced significantly over 48 hours and that the alternate pathway will persist in TUC-3 cells possibly explaining their phenotypic reversion. We will further perform the same experiment with our GST 35-50 peptide. This peptide should block tumor cell growth but not affect levels of the super-complex; rather we anticipate that it will reduce phosphorylation of the kinases in the super-complex. In our animal models, human pancreatic cancer cells (i.e., MIA-PaCa-2 and PANC-1) will be transplanted in the midline of the back (upper thoracic) of nude mice. At an adjacent site, we will implant Alzet pumps that will administer two different concentrations of each peptide over a two week period. Concurrently, we will treat one set of the nude mice with transplanted tumors with a control peptide, PNC-29, that has no effect on pancreatic cancer cell growth. To test if our anti-pancreatic cancer peptides are tolerated immunologically, we will then perform identical experiments on immunocompetent C57 bl/6 mice (5-6 weeks old). For both sets of experiments, we anticipate that, within 2 weeks, tumors will either undergo eradication or reversion to the untransformed phenotype. We also anticipate minimal toxicity in either the nude or syngeneic mouse tumor models. These preclinical studies will provide important data for developing a novel, non-toxic, targeted approach against pancreatic cancer.

**Summary of Research Completed**

Specific Aim 1 – Progress:

We developed novel peptides (PNC-2, PNC-7, PNC-27) that are derived from parts of ras-p21 that block cell division caused by the mutant ras-p21 protein but have no effect on the normal form of this protein. To evaluate the effects of the peptides PNC-2 and PNC-7 on signal transduction in pancreatic cancer cells, we evaluated jun kinase signaling.

The cultured cells were incubated with the different PNC- peptides at a specific dose. Treated cells were washed, harvested in Phosphate buffered saline (PBS) and lysed in 50mM Tris-HCL (pH 8), 1% NP40, 0.1% SDS, 160mM LiCl and sigma protein inhibitor cocktail (1:200) – RIPA Buffer. The lysates were centrifuged for 3 minutes at 14000 RPM. The extracts were aliquoted and stored at -80C. The cell extracts (500ug) were incubated with 2ug of polyclonal anti-H-Ras (N-20 Santa Cruz Biotechnology), 2ug biotinylated anti-rabbit immunoglobulin (Pierce) and 30uL of 50% slurry of immobilized Neurtravidin biotin binding protein beads. The mixture was rocked at 4C for 18 hours. The beads were washed three times with RIPA buffer, resuspended in 30uL of 2X sample buffer and heated to 95C for five minutes. The protein were resolved in 4-20% polyacrylamide gel (Invitrogen) and analyzed by immunoblotting using monoclonal antibodies for pho-JNK (N-7 Santa Cruz Biotechnology). As shown in Figure 1 Ras-derived peptides PNC-2 (Lanes-8 and 11) and PNC-7 (Lane 12) can alter Jun-kinase phosphorylation.

We also evaluated the effects of the peptides PNC-2 and PNC-7 on the K-Ras super complex in pancreatic cells and normal murine cells from spleen and liver. The same methods of cell extraction and electrophoresis were used as for experiments above. Anti-Raf primary antibody was added at 1:2000 dilution (#554134) in 7mL of TBST containing 0.5% milk and incubated overnight on the shaker. The membrane was washed with TBST and anti-mouse Ig-horse radish

peroxidase secondary antibody was added at 1:4000 dilutions in 10mL TBST containing 1% milk. TBST was used to wash the membrane 3 times and the ECL reagent was used to develop the membrane in the dark room at 15 seconds, 1 minute, 3 minutes, and 6 minutes. As shown in Figure 2, The K-Ras super complex contains more RAF-kinase cancer cells MIAPaCa-2 and Panca-2 (lanes 7 and 9) compared to normal murine cells from spleen (Lane 5) and liver (lane 3).

To determine whether PNC-2, PNC-7, and PNC-27 inhibit pancreatic cancer cell growth we measured cell viability using an MTT assay. In a 24- wells plate, approximately 20,000 cells of MIAPaCa and Panco were added to 400 uL of growth media. The cells were treated with increasing doses of peptides at concentrations: 0 uM, 10 uM, 20uM, 40uM, 80uM, and 160uM. The absorbance was recorded at 570nm. As shown in Figure 3 we demonstrate that PNC-2, PNC-7, and PNC-27 peptides inhibit cell proliferation of MIAPaCa-2 cells in a dose dependent manner.

There was no progress on Aim 2.

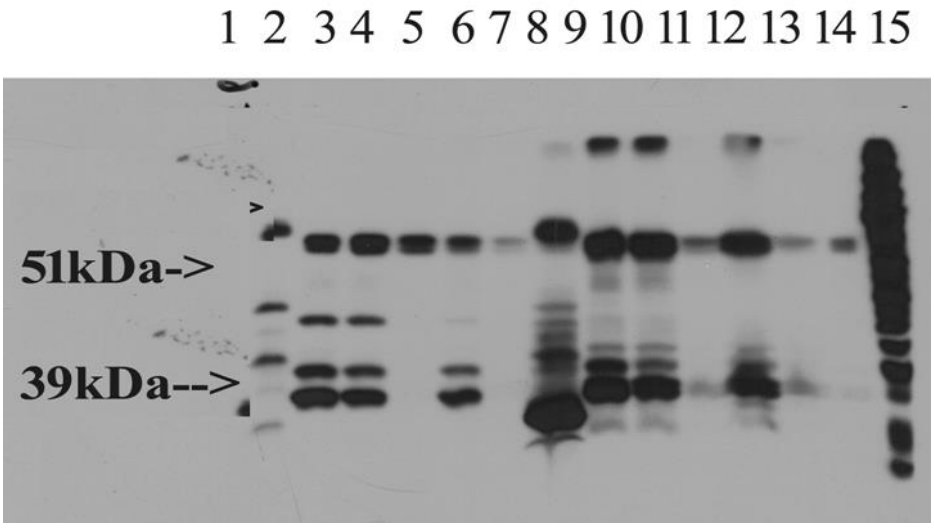


*<u>Figure 1</u>. Immunoprecipitation: H-Ras polyclonal Ab / Western Blots: Anti-phospho JNK polyclonal Ab*

**1**- Protein Ladder; **2**-Panco-2 plasma membrane; **3**- MIAPaCa-2 untreated IP; **4**- Panco-2 untreated IP; **5**- H-Ras Ab; **6**- MCF7 untreated IP; **7**- MIAPaCa PNC 27-24hr IP; **8**- MIAPaCa-PNC2-24hr IP; **9**- MIAPaCa- PNC 29-24hr IP; **10**- Panco-2 PNC 29-24hr IP; **11**- MIAPaCa PNC 2-48hr IP; **12**- MIAPaCa PNC 7-48hr IP; **13**- MIAPaCa extract no primary Ab IP; **14**- MIAPaCa extract no secondary Ab IP; **15**- MIAPaCa total extract no IP

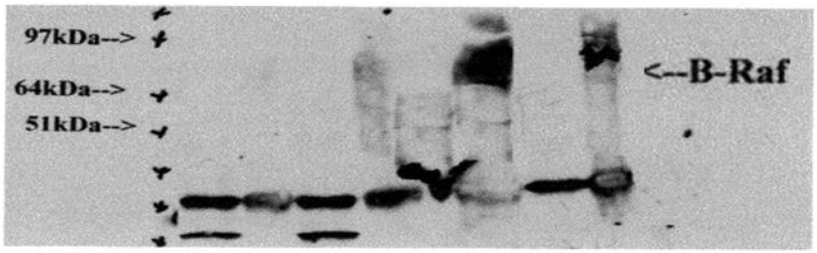


*Figure 2. Immunoprecipitation: K-Ras / Western Blots: Anti-Raf*
**1**- Protein Ladder; **2**- Spleen Total Extract; **3**- Liver IP K-Ras; **4**- Liver Total Extract; **5**- Spleen IP K-Ras; **6**- Panca-2 Total Extract; **7**- Panca-2 IP K-Ras; **8**- MIAPaCa Total Extract; **9**- MIAPaCa-2 IP K-Ras

**MTT Assay- MIAPaCa-2**

| | OD MTT | | | |
|---|---|---|---|---|
| uMpept | PNC-29 | | Average | StandDev |
| 0 uM | 1.472 | 1.472 | 1.572667 | 0.071182 |
| 10 uM | 1.509 | 1.509 | 1.572667 | 0.045019 |
| 20 uM | 1.543 | 1.543 | 1.572667 | 0.020978 |
| 40 uM | 1.645 | 1.645 | 1.572667 | 0.041166 |
| 80 uM | 1.666 | 1.666 | 1.572667 | 0.065997 |
| 160 uM | 1.601 | 1.601 | 1.572667 | 0.020035 |

| uMpept | PNC-27 | PNC-2 | PNC-2 | PNC-29 |
|---|---|---|---|---|
| 0 uM | 1.521 | 1.462 | 1.614 | 1.472 |
| 10 uM | 1.503 | 1.419 | 1.624 | 1.509 |
| 20 uM | 1.602 | 1.593 | 1.608 | 1.543 |
| 40 uM | 0.594 | 1.57 | 1.272 | 1.645 |
| 80 uM | 0.523 | 1.401 | 0.701 | 1.666 |
| 160 uM | 0.296 | 0.471 | 0.431 | 1.601 |

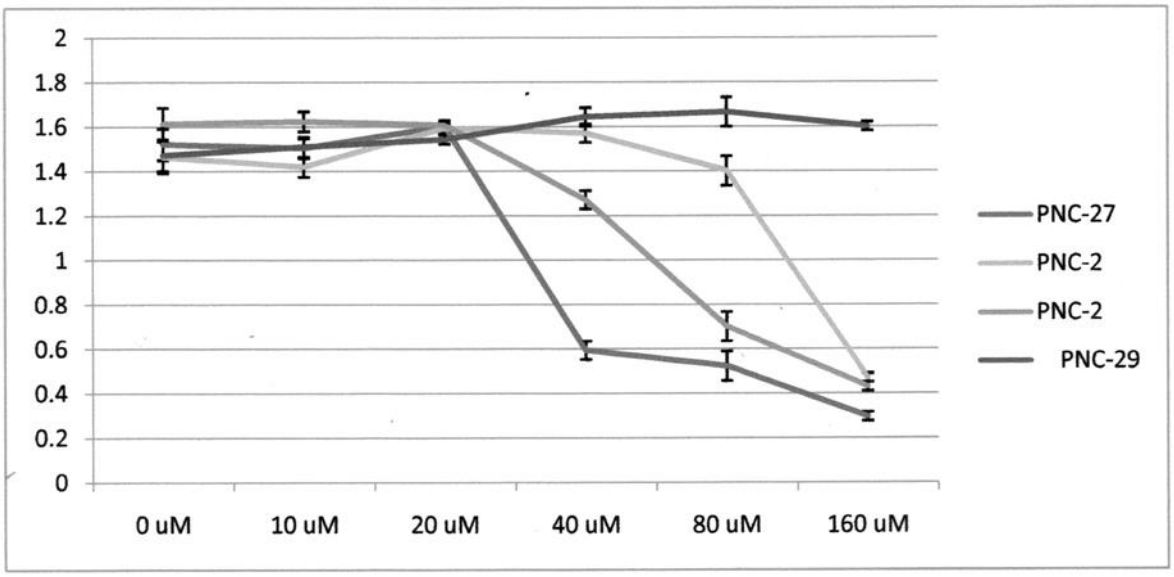


*Figure 3. MTT Assay-*
MIAPaCa-2 cells were treated with increasing doses of peptides at concentrations: 0 uM, 10 uM, 20uM, 40uM, 80uM, and 160uM and viability was determined.

**Research Project 3: Project Title and Purpose**

*Impaired T Cell Immunity and Survival in Neonatal Influenza Virus Infection* – In order to simulate more closely neonatal infection and determine the neonatal responses to viral infection, we have developed a neonatal mouse model to examine acute influenza infection at day 2-3 of life. Preliminary data shows that the neonatal C57Bl/6 mice exhibit significant mortality compared to adult mice. The specific aims of this project are to: 1) determine the mechanism of increased mortality in viral pulmonary infection of neonatal mice and 2) investigate influenza virus-specific CD8+ T cell responses in neonates.

**Duration of Project**

1/1/2012 – 12/31/2013

**Project Overview**

The mortality rate from influenza infection is highest in infants less than the age of six months, which is currently an age group which is not eligible for the available influenza vaccine. There is little data on what precisely leads to immature immune responses and why neonates exhibit increased mortality to influenza virus, if they do not have the mature, full repertoire that adults have at their disposal. The bulk of the current research uses an adult animal model to investigate neonatal infection, so we have established a model of neonatal influenza virus infection that utilizes day 3 old neonatal mice. We hypothesize that the lung environment in the neonatal host responds inappropriately to influenza virus infection producing low amounts of type I IFN and high levels of inhibitory cytokines which lead to increased cytopathic effect of the virus and inhibition of primary and memory CD8+ T cell responses. The specific aims are:

*Aim 1: Examine the influenza virus-specific primary and secondary CD8+ T cell response in neonates.* We have found that when day 3 neonatal C57Bl/6 mice are infected with influenza virus they mount a greatly reduced lung $NP_{366}$-specific CD8+ T cell response on day 10 compared to adult mice, and the neonate response continues to rise at day 14, while the adult response contracts. We will examine later time points of the primary response to confirm the delayed kinetics of the primary response in neonates. Given the greatly reduced primary response, we expect that memory generation will be compromised in neonates. Memory CD8+ T cell responses will be examined on day 60 post infection by tetramers and peptide stimulation combined with ICS. Secondary responses will be determined by heterosubtypic rechallenge of mice on day 60 postinfection with the H3N2 X31 recombinant strain.

*Aim 2: Determine whether the neonatal CD8+ T cell expansion defect is intrinsic or extrinsic.* The initial experiments will focus on whether defects of primary and memory influenza virus–specific CD8+ T cells in neonates are intrinsic to the neonatal CD8+ T cells, or extrinsic and due to the neonatal environment. We will identify the mechanism behind the failure to mount a CD8+ T cell response in neonates.

**Principal Investigator**

Alison J. Carey, MD
Assistant Professor of Pediatrics
St. Christopher's Hospital for Children
3601 A Street
Division of Neonatology
Philadelphia, PA 19134

**Other Participating Researchers**

Peter D. Katsikis, MD, PhD – employed by Drexel University College of Medicine

**Expected Research Outcomes and Benefits**

Each year influenza viruses cause significant morbidity and mortality in neonates. Influenza virus infection is particularly dangerous during the first few months of life, with high hospitalization rates and associated mortality. The studies in this project will elucidate very early events during neonatal influenza virus infection. We are hypothesizing that it is not virus-mediated pathology that is responsible for the neonatal morbidity, but most likely virus-triggered innate cell activation that is the major factor in the morbidity of influenza virus infected neonates. In addition, we expect that the major inhibitory effect is extrinsic to the CD8+ T cells, so that if "normal" adult CD8+ T cells are injected into neonatal mice, there will still be a defective response. We have shown that primary CD8+ T cell responses are reduced in neonates, and we expect neonates will also exhibit reduced memory and secondary CD8+ T cell responses. We suspect this is due to the neonatal cytokine environment. Once we have data on the neonatal mouse response, we can then begin to look at the human neonatal response to many other viral pathogens in both acutely infected and in recovered infants (less than 1 year of age). This knowledge may allow us to develop novel therapeutic strategies against viral respiratory

infections that reduce morbidity and mortality in neonates, accelerate viral clearance and enhance the generation of memory CD8+ T cell responses that can protect from re-infection.

**Summary of Research Completed**

Goals met during this award period:

- Determine the quantity and quality of the memory T cell population after a secondary infection.
- Determine the dominant and subdominant epitope response in the 3-day versus the 7-day old neonate. This also establishes the validity of the 3-day neonatal mouse as a model of failed T cell immunity in neonates.
- Identify the mechanism behind the failed primary response in neonates.

*Methods:*

*Mice and infections*

Experienced timed pregnant female C57Bl/6 mice were purchased to generate neonatal mice and 8 week old adult C57BL/6 mice were purchased from Charles River Laboratory. Animal work was carried out according to approved Institutional Animal Care and Use Committee protocols. Neonatal mice at 3 days of age (weight ~3gr) were infected intranasally (i.n.) with 0.12 $TCID_{50}$ (0.04 $TCID_{50}$ /g) of influenza virus H1N1 strain PR8 (A/Puerto Rico/8/34) (generous gift of Dr. W. Gerhard, Wistar Institute, Philadelphia, PA) in a 5µl volume. Adult 8 week old C57Bl/6 mice (weight ~20gr) were infected i.n. with a sublethal dose of 3 $TCID_{50}$ in a 20µl volume (0.15 $TCID_{50}$ /g). The mice were anesthetized with inhaled isoflurane before intranasal inoculations. For secondary infections, neonatal mice were infected intranasally (i.n.) with 0.08 $TCID_{50}$ of influenza virus H1N1 strain PR8. The adult mice were infected as above with H1N1 PR8 virus. Sixty days later, the mice were challenged with H3N2 X31 recombinant strain.

*Isolation of pulmonary lymphocytes and Flow cytometry*

Pulmonary lymphocytes were isolated from individual mice by removing lungs and mincing into smaller pieces. The tissue was then digested for 2 h at 37°C with 3.0 mg/ml collagenase A and 0.15 µg/ml DNase I (Roche) in RPMI 1640 (Mediatech) containing 5% heat-inactivated FBS (Life Technologies), 2 mM l-glutamine, 100 IU/ml penicillin, 100 µg/ml streptomycin (Mediatech). The digested tissue was then run through a 40-µM cell strainer (Falcon) and washed in the same media as above. Cells were counted using trypan blue exclusion with light microscopy. Influenza virus nuclear protein $(NP)_{(366–374)}$-specific $CD8^+$ T cells were detected using MHC class I tetramers. All surface stains were done on ice to prevent internalization. Cells were fixed in 1% paraformaldehyde (Fisher Scientific) before flow cytometric analysis. Data was collected on a FACS Calibur using Cell Quest software or a FACS Aria using FACS Diva software (BD Biosciences). Analysis was performed using Flow Jo software (Tree Star).

*Subdominant peptide stimulation and Intracellular Cytokine Staining*

The H2K or H2D epitopes associated with these peptides are identified as $D^bNP_{366}$, $D^bPA_{224}$, $K^bNS2_{114}$, and $K^bM1_{128}$ (the immunodominant and subdominant epitopes in influenza infection in the B6 mouse). The peptide stimulation assay used isolated pulmonary lymphocytes incubated for 5 hours at a concentration of $2 \times 10^6$ cells in 200 µl of RPMI 1640 medium containing 10% FBS, and 5 µg/ml Brefeldin A (Epicentre Technologies, Madison, WI) in the

presence or the absence of 1 μM viral peptide. The T cells were then washed and stained with anti-mouse CD8α-PE Ab (eBioscience, San Diego, CA). The cells were permeabilized in PBS/0.5% saponin for 20 min before staining with mouse IFN-γ-APC (Tonbo Biosciences). Isotype control Antibody was also used. Cells were fixed in 1% paraformaldehyde (Fisher Scientific) before flow cytometric analysis.

*Cell Sorting and TCR sequencing*

Lymphocytes were isolated from the lungs of influenza A infected newborn and adult mice on day 10 of infection. Influenza virus nuclear protein $(NP)_{(366–374)}$-specific $CD8^+$ T cells were detected using MHC class I tetramers. Cells were stained on ice for 40 min with anti-mouse CD8α conjugated to PE (Tonbo Bioscience, San Diego CA) and $NP_{(366–374)}$-specific tetramer. Tetramers were prepared with APC-labeled streptavidin (Molecular Probes). Cells were washed once, counted and re-suspended in HBSS with 3% FBS at a concentration of $20 \times 10^6$ cells/ml. $NP_{(366–374)}$-specific CD8+ T cells were then sorted on a FACSAria™ fluorescence-activated cell sorter (BD Biosciences). gDNA extraction was performed following the DNeasy Blood and Tissue Kit (Qiagen). Samples were analyzed with high-throughput sequencing of the TCR V-beta CDR3-region with the Illumina Genome Analyzer from Adaptive Biotechnologies using the ImmunoSeq® immune-profiling system at the survey level, designed to target an output of 200,000 assembled output sequences. Sorted cell numbers ranged from ~10,000 to ~100,000, assuring at least 5-fold depth of sequencing.

*Statistical analysis:*

Statistical analysis was performed using the Shapiro-Wilk W test for normality, Student's t-test and nonparametric Wilcoxon signed-rank test for paired and unpaired samples. Nonparametric (Spearman's rho) statistics were used for measurements of correlation. Analyses were performed with the JMP statistical analysis program (SAS, Cary, NC). P values$<0.05$ were considered to be statistically significant.

*Results:*

*Comparison of the 3-day old neonate and the 7-day old neonate*

It has been reported in the literature that neonatal mice at 6-7 days of age can develop a more varied cytotoxic T cell response to respiratory viral pathogens, whereby there can be an expansion of viral specific $CD8^+$ T cells specific for subdominant epitopes. We infected neonates at 3 days of age, neonates at 7 days of age, and adult mice with influenza, to identify the T cell hierarchy in both the 3-day old mouse and the 7-day old mouse. At day 10 post-infection, which is the height of the primary response, animals were harvested and peptide stimulations and intracellular staining were performed to determine the dominant and subdominant response. Both groups of neonates had a depressed $NP_{366–374}$ response in terms of absolute numbers ($3.1 \times 10^4 \pm 0.9$ (3-day) and $4.1 \times 10^4 \pm 1.0$ (7-day) per 100 mg lung tissue) versus the adult controls ($18.2 \times 10^4 \pm 4.4$ per 100 mg lung tissue), indicating that regardless of age of infection the dominant response is inadequate (Figure 1A). However, the response to other epitopes is quite different between the 7-day old neonate and the 3-day old neonate. The 7-day old neonate has a subdominant response similar to the adult. For $PA_{224–233}$ which is another dominant epitope in the mouse, the 3-day old mouse has a depressed response in terms of absolute numbers ($3.5 \times 10^4 \pm 0.9$ per 100 mg lung tissue) versus the other 2 groups ($15.3 \times 10^4 \pm 3.8$ (7-day) and $18.5 \times 10^4 \pm 3.3$ (adult) per 100 mg lung tissue) (Figure 1B). For the subdominant

epitope to the matrix protein $M_{128–135}$, the 3-day old mouse has a depressed response in terms of absolute numbers ($3.5x10^4$±0.9 per 100 mg lung tissue) versus the other 2 groups ($14.3x10^4$±3.2 (7-day) and $26.9x10^4$±5.9 (adult) per 100 mg lung tissue) (Figure 1C). For the subdominant epitope to the nonstructural protein 2 ($NS2_{114–121}$), the 3-day old mouse has a depressed response in terms of absolute numbers ($0.1x10^4$±0.1 per 100 mg lung tissue) versus the other 2 groups ($14.4x10^4$±4.7 (7-day) and $6.3x10^4$±2.6 (adult) per 100 mg lung tissue) (Figure 1D). These results demonstrate two points. First, the 3-day old neonate is not expanding a different clone of viral specific T cells than the standard $NP_{366–374}$ clone in order to combat the infection. There is a global depression of the expansion of multiple types of viral specific T cells. Second, the 7-day old mouse has a similar response to the $NP_{366–374}$ dominant peptide as the 3-day old mouse. However, the 7-day old mouse is able to develop a subdominant response to influenza, indicating the development of greater TCR diversity over the first week of life.

*Mice infected during the neonatal period have a robust secondary $CD8^+$ T cell response.*
Since neonatal mice had a reduced and delayed primary virus-specific T cell response to infection, we wanted to determine if mice infected as neonates could establish memory and mount an appropriate secondary response to influenza virus infection. In adult mice, the secondary $NP_{(366-374)}$-specific $CD8^+$ T cell response to influenza virus in the lung peaks on day 7-8 with a frequency of 30% of the $CD8^+$ T cells. We found that secondary responses in mice that were neonates during primary infection did not differ from those of adult mice. Secondary lung $NP_{(366-374)}$-specific $CD8^+$ T cell responses in mice primed as neonates were similar in magnitude to those of mice primed as adults in both frequencies (26.6%±4.8 versus 39.5%±5.1 of lung $CD8^+$ T cells, respectively) (Figure 2A and B) and numbers ($1.8x10^6$±0.7 versus $1.4x10^6$±0.5 $NP_{(366-374)}$-specific $CD8^+$ T cells per 100mg of lung, respectively) (Figure 2C). In order to test the quality of this memory cell population, we performed a peptide stimulation with the immune-dominant peptide $NP_{(366-374)}$, and found that the absolute numbers of IFN gamma producing CD8+ T cells are similar between animals infected the first time as a neonate versus those animals infected for the first time as adults, when exposed to the immune-dominant peptide $NP_{(366-374)}$ ($5.1x10^5$±1.4 versus $1.4x10^5$±0.3) (Figure 2D). Next, we performed viral loads (Figure 2E). Viral loads are similar between those animals who received a primary infection in the neonatal period versus those animals who received a primary infection as an adult, further indicating that the quality of the memory response is similar in animals infected as a neonate. Thus, in spite of a defective primary response in neonates, these animals can establish memory and mount an intact secondary response.

*Next generation sequencing of the Neonatal versus Adult mouse T cell receptor repertoire*
After finding the neonatal environment was not suppressive and neonatal T cells with a transgenic TCR can expand normally in both the neonate and the adult, we sought to identify differences in the neonatal and adult wild-type TCR repertoire by performing next generation sequencing of sorted, $NP_{(366-374)}$ tetramer positive CD8+ T cells from animals on day 10 post-infection. The top shared adult clones were CASSGGSNTGQLYF, CASSGGANTGQLYF, CASSGGGNTGQLYF, and CASRGGANTGQLYF, which are all clones which have been previously established as public clones in the mouse viral specific immunodominant $NP_{(366-374)}$ response to influenza infection. In contrast, the neonates do not have any of the adult clones. Instead, they demonstrate a pattern of having 2-3 dominant clones which show only some overlap with the other neonatal samples (Figure 3). The adults share high frequency clones. The

neonates share some clones, but not high frequency clones. In addition, there are fewer expanded clones in the neonates. Finally, the CDR3 length is shorter in the neonates, which inherently leads to less diversity.

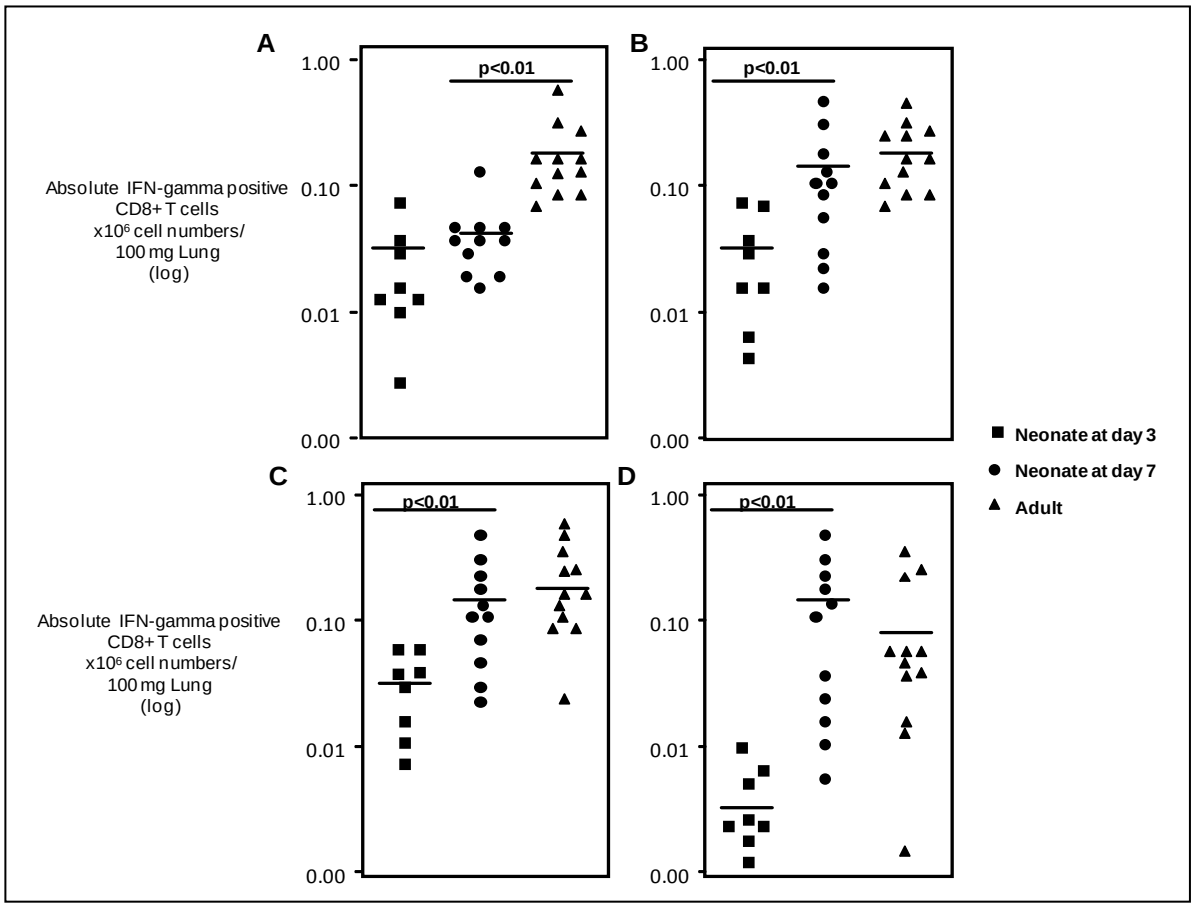


Figure 1: The viral specific CD8+ T cell response in animals infected at 3-days, 7-days, and 8-weeks. **(A)** Pooled data showing absolute numbers of IFN-gamma+/ $CD8^+$ T cells per 100 mg of lung shown from the lungs of day 10 post-infection animals. The lymphocytes were incubated for 5 h in RPMI 1640 containing Brefeldin A (5 μg/ml) in the presence or the absence of the $NP_{366}$ ($H2D^b$) peptide, then fixed and stained for CD8α and IFN-γ. Symbols represent individual animals, with the horizontal line marking the mean of each group (n= 8-12 mice per group). Data are from at least two independent experiments. Absolute numbers of IFN-gamma+/ $CD8^+$ T cells per 100 mg of lung shown from the lungs of day 10 post-infection animals after peptide stimulation with **(B)** $PA_{224–233}$, **(C)** $M_{128–135}$ **(D)** $NS2_{114–121}$.

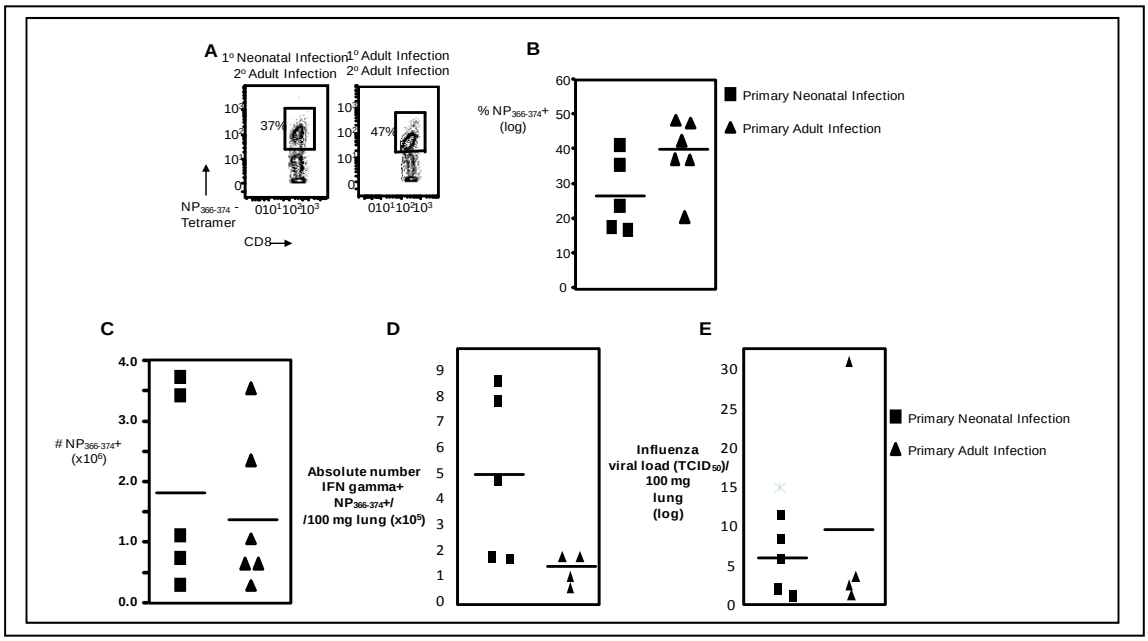


Figure 2**:** Mice infected during the neonatal period have a robust secondary $CD8^+$ T cell response. Primary infection was performed in 3-day old neonatal or adult mice with PR8 influenza. Sixty days after this primary infection, the mice were challenged with H3N2 X31 recombinant strain and viral specific $CD8^+$ T cells were analyzed day 7 post-infection. (A) Representative flow cytometry plots are shown with percentage of $NP_{(366-374)}$-specific $CD8^+$ T cells from mice either infected as neonates or adults and challenged as adults. Pooled data showing percentage (B) and absolute cell numbers (C) of $NP_{(366-374)}$-specific $CD8^+$ T cells. (D) of IFN-gamma positive CD8+ T cells per 100 mg of lung. Viral loads (E) of primarily infected neonates versus primarily infected adults were measured at days 7 post-infection by real-time PCR. Viral loads were normalized per 100 mg of lung tissue. Symbols represent individual animals, with the horizontal line marking the mean of each group (n= 4-6 mice per group). Data are from two independent experiments.

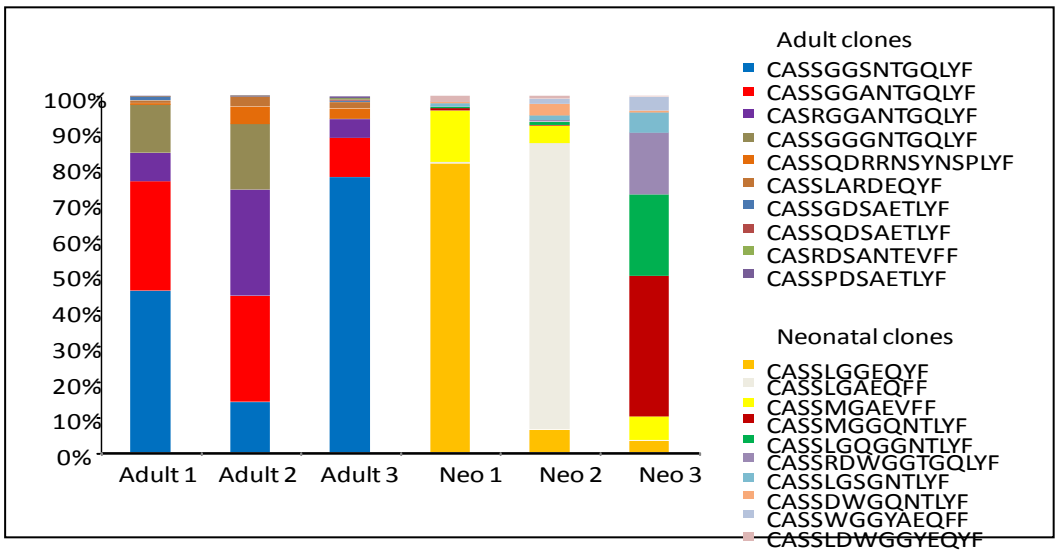


Figure 3: Top ten T cell receptor clones of viral-specific CD8+ T cells in adults and neonates. $NP_{(366–374)}$-specific CD8+ T cells were sorted and next generation sequencing was performed to determine the dominant clones in the influenza response. The top four clones seen in the adult group are shared among the 3 animals, and have been previously described in the literature as public viral-specific CD8+ T cell clones. In contrast, the neonates have expansion of a completely different set of clones, with each animal having a specific clone as their top clone.

## Research Project 4: Project Title and Purpose

*Epigenetic Modulation in an Animal Model of Depression* – The purpose of this project is to understand the neuroadaptive mechanisms that occur in the central nervous system (CNS) in response to chronic inflammation and immune dysregulation and contribute to a depressive behavioral phenotype. We will study a model of chronic inflammation in the mouse where immunization with Bacille Calmette Guerin leads to activation of the innate immune response and the development of a depressive phenotype. We expect that the findings from these studies will suggest novel targets for treating patients with inflammation related Major Depressive Disorder (MDD).

### Duration of Project

1/1/2012 – 6/30/2013

### Summary of Research Completed

This project ended during a prior state fiscal year. For additional information, please refer to the Commonwealth Universal Research Enhancement C.U.R.E. Annual Reports on the Department's Tobacco Settlement/Act 77 web page at http://www.health.state.pa.us/cure.

## Research Project 5: Project Title and Purpose

*Characterization of the Effects of Non-thermal Plasma on Liquids and Cells* – In order to exploit the potential for clinical applications, from enhancing wound healing, to sterilizing tissues, to inducing localized apoptotic cell death in tumor tissue, a mechanistic understanding of the interaction of non-thermal plasma with living tissues is required. Our initial studies using mammalian cells in culture revealed that non-equilibrium plasma (NEP) has dose-dependent effects that range from increasing cell proliferation to inducing apoptosis; these effects are primarily due to formation of intracellular reactive oxygen species (ROS). We propose to study the effect of NEP on molecules in solution and on DNA damage pathways to better understand the biological effects.

### Duration of Project

1/1/2012 – 6/30/2013

### Summary of Research Completed

This project ended during a prior state fiscal year. For additional information, please refer to the Commonwealth Universal Research Enhancement C.U.R.E. Annual Reports on the Department's Tobacco Settlement/Act 77 web page at http://www.health.state.pa.us/cure.

## Research Project 6: Project Title and Purpose

*Novel Antagonists of CX3CR1 to Prevent Skeletal Metastasis* – The overall goals of this proposal are to synthesize the first small-molecule, non-peptide antagonists of $CX_3CR1$ and produce pre-clinical evidence that these compounds, by interfering with $CX_3CR1$-FKN interactions, impair the dissemination of breast cancer cells to the skeleton. We propose a radical switch in the current standard of care for breast cancer patients, with the implementation of systemic therapeutic measures to be started immediately after breast surgery and maintained during the time preceding second surgery or local adjuvant treatments.

### Duration of Project

1/1/2012 – 6/30/2013

### Summary of Research Completed

This project ended during a prior state fiscal year. For additional information, please refer to the Commonwealth Universal Research Enhancement C.U.R.E. Annual Reports on the Department's Tobacco Settlement/Act 77 web page at http://www.health.state.pa.us/cure.

**Research Project 7: Project Title and Purpose**

*Astrocyte Senescence as a Component of HIV-related Neurodegeneration* – Aging of the HIV-infected population places the disease in a distinctive set of biological and psychosocial influences. Our main purpose is to identify common factors and mechanisms in the interplay of aging and HIV. We find that astrocytes enter into senescence in response to oxidative stress and HIV-1 proteins and that the brains of aged individuals and individuals with Alzheimer's disease are highly populated by senescent astrocytes. Because HIV infection is associated with the release of neurotoxic factors which induce cell stress, we plan to evaluate the impact of viral factors on astrocyte senescence. Our studies will provide information for successful therapeutic efforts to alleviate HIV-associated neurocognitive disorders during aging.

**Anticipated Duration of Project**

1/1/2012 – 12/31/2014

**Project Overview**

Aging of the human immunodeficiency virus type 1 (HIV-1)-infected population places HIV/AIDS in the context of aging. One of our research objectives is to identify common factors and mechanisms between aging and HIV. Astrocytes, the most abundant cell type in the brain, perform vital functions in the central nervous system. Astrocytes are host cells for HIV-1 infection and we postulate that changes in astrocyte function may contribute to the neuropathogenesis of HIV-associated neurocognitive disorder (HAND). Recently, we have reported that human astrocytes are highly sensitive and trigger a senescence program in response to oxidative stress or cellular insult. We have evidence indicating that the number of senescent astrocytes increases in the brain with age, and further in patients suffering from Alzheimer's disease. HIV infection is associated with the release of neurotoxic factors, such as HIV-gp120, and we predict that this stressful environment will trigger the senescent program in astrocytes. Preliminarily, we found that HIV-gp120 protein induces astrocyte senescence. We hypothesize that senescent astrocytes negatively impact the microenvironment, contributing to HAND in older patients living with HIV/AIDS.

*Aim 1. Determine the impact of HIV-1 on astrocyte senescence during aging of infected patients. Rationale:* We will perform a comprehensive analysis of brain tissue of patients infected by HIV-1 at different ages. We will quantify senescent astrocytes using a variety of markers of senescence in several brain areas from tissue samples from the National NeuroAIDS Tissue Consortium (NNTC). We will also study effects on neurodegeneration and microglia.

*Aim 2. Evaluate the influence of HIV-1 viral products on the astrocyte senescence program and the secretion of pro-inflammatory mediators. Rationale:* Astrocytes are highly sensitive and we hypothesize that viral products trigger the senescent program. We will evaluate effects of HIV-1 gp120 /Tat proteins on astrocyte senescence, and the secretory pattern. In addition, we will evaluate effects of pharmacologic intervention to block senescence, by inhibiting mTOR and p38MAPK. These targets will provide preclinical data for further testing models or pharmaceuticals to block senescence associated cellular changes that affect neural physiology.

**Principal Investigator**

Claudio A. Torres, PhD
Assistant Professor
Drexel University College of Medicine
245 N. 15th Street
Philadelphia, PA, 19102

**Other Participating Researchers**

Liz Crowe, BS; Christian Sell, PhD; Michael Nonnemacher, PhD; Brian Wigdahl, PhD – employed by Drexel University College of Medicine

**Expected Research Outcomes and Benefits**

Based on our data indicating that human astrocytes trigger the senescent program in response to a variety of stressors in vitro, the increased population of senescent astrocytes in brain tissue during aging and Alzheimer's disease, and our results showing the ability of viral products such as HIV-1 gp120 to induce astrocyte senescence; we expect to find a significant increase in the population of senescent astrocytes in human brain of patients infected with HIV-1. HIV infection is associated with a stressful environment including the release of neurotoxic factors, oxidative stress, and inflammation, favorable conditions that could trigger the senescent program in astrocytes and create a loss in homeostasis in the CNS. We anticipate that the amount of senescent astrocytes will be higher in older HIV-1-infected patients compared with younger HIV-1 infected patients. We anticipate finding a higher abundance of senescent astrocytes, neurodegeneration and microglia activation in those areas preferentially affected by HIV-1 infection. We assume that the pattern of gene expression and biomarkers of senescence altered during *in vitro* astrocyte senescence will be similarly affected in brain tissue during HIV-1 infection.

Viral products such as HIV-1 gp120 and tat induce oxidative stress and inflammation in astrocytes. Given this, we hypothesize that they will induce the expression of markers of senescence and an altered secretion pattern including releasing of cytokines, proteases, and reactive oxygen species. We propose mTOR and p38MAPK as target pathways of the HIV-1-induced astrocyte senescence, and we anticipate that pharmacologic intervention to block these pathways will modulate senescence, reduce the secretion pattern of astrocytes, influence neural physiology and be potential therapeutic targets to improve HAND during the aging of these patients.

**Summary of Research Completed**

*Aim 1. Determine the impact of HIV-1 on astrocyte senescence during aging of infected patients.*

Post-mortem frontal cortex sections from age-matched HIV+ subjects with and without HIV associated dementia (HAD) were probed with antibody to IL-6 in order to assess the extent of inflammation. In a preliminary analysis for each case, interleukin-6 (IL-6) positive (cytoplasmic or extracellular brown stain) and negative cells were counted from 3 different areas from each slide (Fig. 1A). IL-6 staining was higher in the apex of the cortex for the non-HAD case, and in

longitudinal and basal cross-sections for the HAD case (Fig. 1B). Overall, there was a slightly greater percentage of IL-6 positive cells in the FC tissue from the HIV patient with HAD compared to the patient without HAD (Fig. 1C).

While a comprehensive study is necessary to evaluate the differences in IL-6 secretion and overall inflammation in HIV associated dementia and neurocognitive disorders, these results indicate a possible region specific difference in IL-6 secretion in HAD. Moreover, the high IL-6 staining in the HIV+ subject without dementia may be contributed to by ongoing viral replication, and may precede HAD. Thus a comparison to an HIV- subject is necessary to distinguish the effects of HIV at different stages of neurocognitive disorder.

*Aim 2. Evaluate the influence of HIV-1 viral products on the astrocyte senescence program and the secretion of pro-inflammatory mediators.*

We have analyzed the effect of several HAART drugs on the senescence program of human astrocytes. Pre-senescent human astrocytes were treated with ritonavir, an HIV-protease inhibitor, and the reverse transcriptase inhibitors tenofovir and emtricitabine. Our results indicate that compared to untreated controls, ritonavir and reverse transcriptase inhibitors were able to induce a significant increase in the activity of the senescence marker beta galactosidase (Figs. 2A, B). Interestingly, pretreatment with rapamycin, a specific mTOR inhibitor, was able reduce the percent of senescence astrocytes, suggesting that rapamycin could be used as a potential intervention to mitigate the senescence induced by HAART in human astrocytes. In further studies we have demonstrated that HAART-induced senescence was accompanied by an altered pattern of secretion known as the senescence-associated secretory phenotype (SASP). As shown in figure 2C ritonavir induced the secretion of several factors, including pro-inflammatory cytokines. This suggests that senescent astrocytes may represent a significant contributor to the chronic inflammatory response observed HIV patients under HAART.

In addition we have initiated studies with nucleotide reverse transcriptase inhibitors (NRTIs) abacavir (ABA) and lamivudine (3TC) both with satisfactory brain penetrance. Human astrocytes were treated with abacavir, lamivudine or both for up to 2 weeks in complete astrocyte media. These drugs affected the replicative capacity of astrocytes (Fig. 3A), and induced beta galactosidase activity (Figs. 3B,C). In addition, abacavir/lamivudine-induced senescence was accompanied by the generation of oxidative stress, as indicated by increased production of total and mitochondrial reactive oxygen species (ROS) (Figs. 4A,B), and increased level oxidized molecules as indicated by an increase in protein carbonyl content (Fig. 4C). These results suggest that abacavir and lamivudine may affect mitochondrial function. In addition, we have demonstrated that by induction of astrocyte senescence by these drugs may play a critical role in the chronic inflammatory process observed in HIV-infected patients, as suggested by increases in IL-8 mRNA level and in NF-κB activity (data not shown).

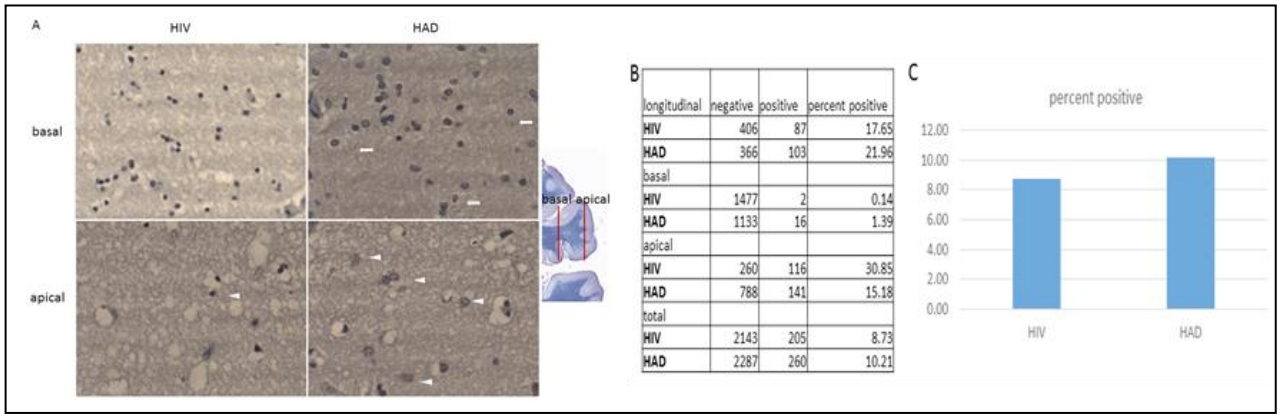


Fig. 1. (A). Frontal cortex sections of age matched HIV+ subjects without neurocognitive decline and with HIV associated dementia (HAD) were stained with antibody to IL-6 (brown) and hematoxylin for DNA (blue). Sample images from basal and apical cross sections are shown. Inset: Diagram depicting the path of images taken from the sections for the basal and apical image sets. (B). Counts of cells without (negative) and with (positive) brown staining for IL-6. Image sets taken in apical and basal directions and in a direction crossing both apical and basal domains (longitudinal) were counted. (C). Graphical representation of the total percentage of IL-6 positive cells from the combined image sets.

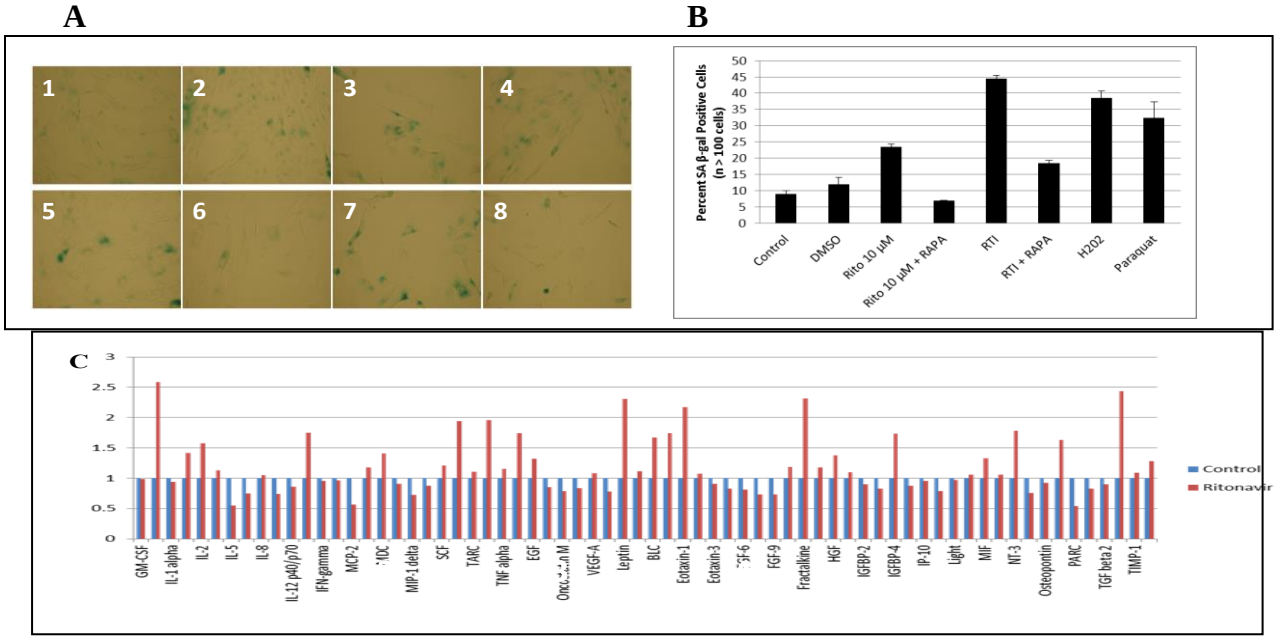


Fig. 2. Effects of HAART on astrocyte senescence. (A) 1. Control. 2. DMSO. 3. $H_2O_2$ 200 μM, 2 hours. 4. Paraquat 150 μM, 24 hours. 5. Ritonavir (Rito)10 μM, 6. Rapamycin (RAPA) 10 nM + Rito 10 μM. 7. Reverse transcriptase inhibitors (RTI) Tenofovir + Emtricitabine 40 μM. 8. RAPA10 nM + RTI. With the exception of $H_2O_2$ and Paraquat, astrocytes were treated for a period of 5 days with a second dose administered 48 h after the first. RAPA was administered 48 h prior to Rito or the RTIs. Cells were then stained for SA β-gal. (B) % of SA β-gal expressing cells. (C) Senescence-associated secretory phenotype. Cells were treated for a week as described in complete astrocyte media. Secreted factors were then collected in MCBD-105 media for 48 hrs. Conditioned media was analyzed using an antibody array (Raybiotech).

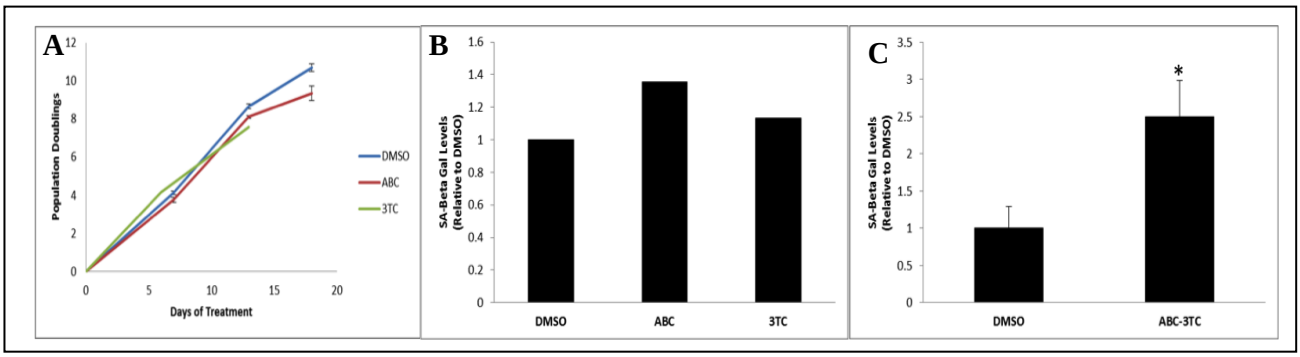


Fig. 3. Effect of abacavir and lamivudive on astrocyte senescence. Human astrocytes were treated with 3μM abacavir (ABC), 1.9 μM lamivudine (3TC), or both for up to 2 weeks in complete astrocyte media. (A) Growth inhibition curves. (B-C) SA β-gal activity: cells were stained for SA β-gal after 1 week of HAART treatment and the fraction of positive cells were displayed as a ratio relative to DMSO controls. * = p value < .05, error bars represent the mean of 3 biological replicates

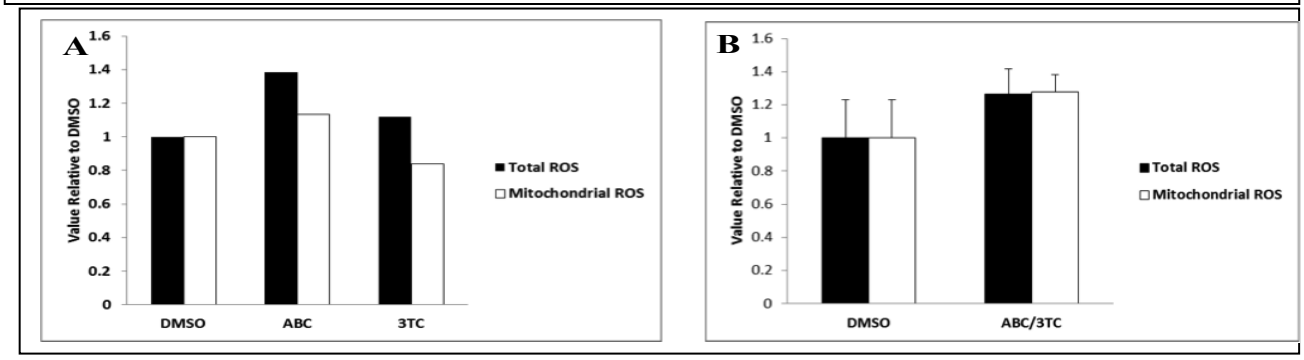


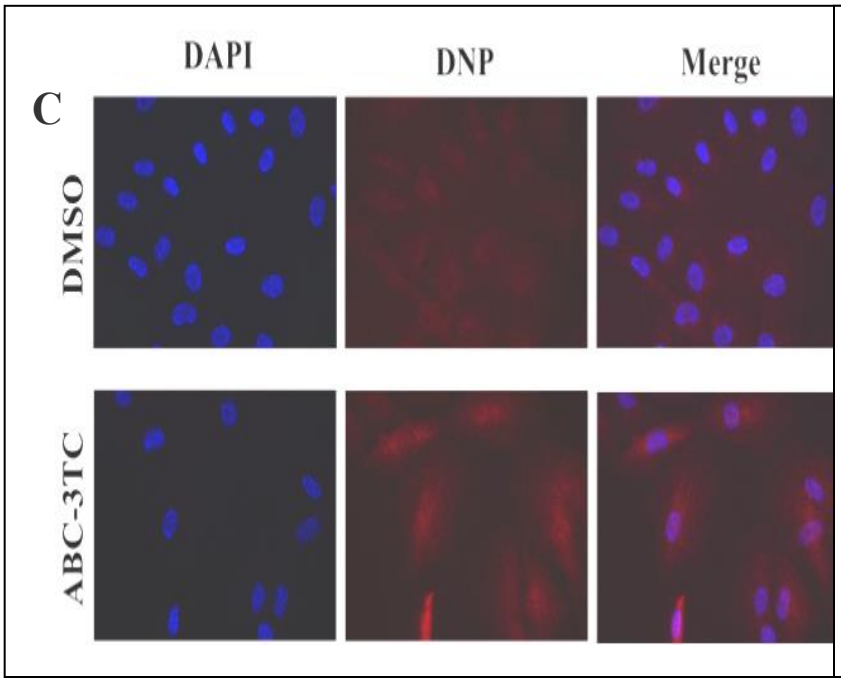


Fig. 4. Effect of abacavir and lamivudive on oxidative stress. Human astrocytes were treated with ABC and 3TC (A) or ABC-3TC co-treatment (B), as indicated above. Cells were stained with either DCFDA (total ROS) or MitoSox (mitochondrial ROS) for 30 min and fluorescent measurement of reactive oxygen species was performed by flow cytometry. (C). Oxidative damage of ABC-3TC co-treatment. Cells were permeabilized on coverslips before incubation with 2,4 Dinitrophenol hydrolase (DNPH) for 15 min. The cells were then blocked with 5% goat serum in 0.1%-BSA-PBS for 2 hrs before overnight incubation with DNP antibody. Shown are representative microscopy images at 40X.

## Research Project 8: Project Title and Purpose

*Aβ Peptide and Vascular Dysfunction in Alzheimer's Disease* – Vascular dysfunction occurs in Alzheimer's disease, however, the role of vascular dysfunction in Alzheimer's disease initiation and progression is not known. Furthermore, the effect of the mechanical environment on brain microvascular endothelial cells has not been extensively studied. This project will determine the effect of Aβ peptide on vascular endothelial cell response to fluid shear stress and angiogenesis. While current medications can slow the progression of dementia symptoms, there are currently no treatments to prevent, halt, or cure Alzheimer's disease. These fundamental studies will elucidate new roles for Aβ peptide and the microvasculature in the disease, and lead to new targets for pharmaceutical therapies.

### Duration of Project

1/1/2012 – 6/30/2013

### Summary of Research Completed

This project ended during a prior state fiscal year. For additional information, please refer to the Commonwealth Universal Research Enhancement C.U.R.E. Annual Reports on the Department's Tobacco Settlement/Act 77 web page at http://www.health.state.pa.us/cure.

## Research Project 9: Project Title and Purpose

*Interactive Roles of Interstitial Flow and Hepatitis B Virus in Liver Cancer Progression* – The purpose of the project is to determine how interstitial flow affects the invasive behavior of primary liver cancer cells, and whether this process is potentiated by hepatitis B infection. Liver cancer is one of the most common cancers worldwide, resulting primarily from chronic hepatitis B infection, and incidence in the United States is rising. The processes underlying the link between liver cancer and hepatitis B remain poorly understood. At the same time, the role of biomechanical forces in cancer progression is increasingly being appreciated. Our project will elucidate interactions between biomechanical forces and hepatitis B infection to understand their contributions to liver cancer invasion, and develop targeted therapies to halt these processes.

### Duration of Project

1/1/2012 – 12/31/2013

### Project Overview

Our overall objective is to elucidate how interstitial fluid flow interacts with hepatitis B virus (HBV) infection in promoting hepatocellular carcinoma (HCC) progression. The central questions addressed by this project are *"What is the mechanism of interstitial fluid flow-induced invasion of hepatocellular carcinoma cells, and does hepatitis B virus switch on this mechanism in hepatocytes?"* To answer these questions, we propose two specific aims:

Specific Aim 1—Determine the mechanism of interstitial fluid flow-induced invasion of hepatocellular carcinoma cells: Using human cell lines and primary rat hepatocytes, we will determine the effect of interstitial flow on HCC cell invasion, and elucidate the underlying mechanisms driving this process. Our hypothesis is that HCC cells that express high levels of the chemokine CXCL12 and its receptor CXCR4 will invade due to "autologous chemotaxis", where interstitial flow alters transport of chemokines, resulting in pericellular chemokine gradients. To test this hypothesis, we will use a 3-D invasion assay incorporating interstitial flow and inhibition of chemokines and chemokine receptors (via pharmacological inhibitors and RNA interference). We will also elucidate the intracellular signaling pathways activated by interstitial flow and link these to observed changes in HCC cell behavior.

Specific Aim 2—Elucidate the effects of an HBV infection on the response of hepatocytes to interstitial fluid flow: We will measure how infection of hepatocytes with HBV, in particular the expression of the HBV X protein (HBx), affects the ability of hepatocytes to respond to interstitial flow. Our hypothesis is that HBV infection of hepatocytes induces concurrent and elevated expression of CXCL12 and CXCR4, conferring on the cells the ability to sense and invade in response to interstitial flow. To determine the effects of HBV on flow-mediated hepatocyte invasion, we will use cell lines that express HBV proteins or primary rat hepatocytes transfected with hepatitis B viral DNA. We will then quantify the invasive behavior and expression of chemokines, chemokine receptors, and signaling pathways identified in Aim 1.

**Principal Investigator**

Adrian C. Shieh, PhD
Assistant Professor
Drexel University
3141 Chestnut Street
Philadelphia, PA 19104

**Other Participating Researchers**

Michael Bouchard, PhD – employed by Drexel University College of Medicine

**Expected Research Outcomes and Benefits**

As liver cancer incidence and mortality rises in the United States, there is an increasing need to better understand disease progression. Because chronic hepatitis B virus (HBV) infections remain the most common cause of hepatocellular carcinoma (HCC), accounting for at least 50 – 60% of reported cases, understanding processes that link HBV infection to HCC development remains critically important. In addition, a more general understanding of processes associated with the development of HCC may provide insights into mechanisms that link metabolic syndrome and fatty liver disease to the development of HCC.

To address this need, the project works at the interface of biomedical engineering, physical sciences, and cell biology, asking how molecular factors such as HBV infection interact with physical factors like interstitial fluid flow to promote the progression of HCC. Key expected

outcomes will include elucidating the molecular factors that promote interstitial flow-mediated liver cancer cell invasion, and the role of HBV protein expression in modulating that invasion. Furthermore, the results of the project have the potential to introduce a new paradigm into our understanding of HCC – that of the significant involvement of biomechanical forces and their interactions with liver cell biology and pathobiology. By identifying key molecular factors involved in liver cancer progression, we will contribute to improved diagnosis and targeted therapies that can combat the most invasive of liver cancers.

**Summary of Research Completed**

The overall objectives of the project are to determine the mechanism of interstitial flow-induced hepatocellular carcinoma cell invasion, and elucidate the role of hepatitis B viral infection in modulating this mechanism. For this reporting period, our primary goal was to determine the mechanism of interstitial flow-induced hepatocellular carcinoma (HCC) cell invasion and quantify the effects of hepatitis B virus (HBV) protein expression on the flow response of HCC cells. To date, we have determined that interstitial flow-induced HCC cell invasion occurs through a CXCR4/CXCL12-dependent mechanism that requires a CXCL12 gradient. Furthermore, activation of MEK1/2 is also necessary for flow-induced invasion, though our results suggest that MEK1/2 is not downstream of CXCR4/CXCL12, and thus modulates invasion through another, currently unknown mechanism.

Methods

*Cells:* A panel of cell lines was used for the studies, including Huh7 human hepatoma cells, Hep3B human hepatoma cells with an integrated HBV genome, HepG2 human hepatoblastoma cells, and primary rat hepatocytes (PRHs). Cell lines were maintained using line-specific cell culture conditions; PRHs were used immediately post-isolation to minimize hepatocyte dedifferentiation caused by *in vitro* culture. To test the role of HBV in the response of HCC cells to interstitial flow, Huh7 cells were transfected with the empty pGEM plasmid or a plasmid containing HBV DNA (pGEMHBV).

*3-D invasion assay:* HCC cells were encapsulated in a 1.3 mg/ml type I collagen gel (rat tail tendon-derived; BD Biosciences) supplemented with 1 mg/ml Matrigel reconstituted basement membrane matrix (BD Biosciences) at a cell density of $5 \times 10^5$ cells/ml. The cells were seeded inside transwell culture inserts (Millipore) with 8 μm diameter pores to allow for cell migration across the lower membrane. The number of cells that migrated through the membrane was used as a metric to quantify liver cancer cell invasion in response to interstitial fluid flow. Interstitial flow was induced by imposing a pressure head across the gel, driving fluid flow through the gel in the direction of the membrane. While the fluid flow velocity varies, we estimate that it is ~0.1 μm/s. Static control transwells had balanced fluid levels to minimize interstitial flow. All 3-D invasion experiments lasted 24 h. At the end of the experiment, the number of invaded cells was counted and invasion was calculated as a percentage of the original cell number seeded.

To determine the role of CXCL12 in interstitial flow-induced Huh7 invasion, two different experiments were performed. First, a neutralizing antibody against CXCL12 (R&D Systems, Minneapolis, MN) was incorporated into the 3-D invasion assay to specifically block CXCL12 activity. Second, a high (80 ng/ml), uniform concentration of CXCL12 was incorporated into the

medium and matrix of the 3-D invasion assay. If a gradient of CXCL12 is necessary, as hypothesized by the autologous chemotaxis mechanism, saturating the system should ablate the gradient. To determine the role of MEK1/2 activation in interstitial flow-induced Huh7 invasion, the small molecular inhibitor U0126 was incorporated into the 3-D invasion assay at a concentration of 25 μM.

*Western blot:* Western blot was used to measure levels of total and phospho-proteins. Protein was acquired by lysing cells with radioimmunoprecipitation assay (RIPA) buffer with protease inhibitor cocktail. For 3D samples, cells were first digested out of the gels with collagenase D (10 mg/ml) for 45 minutes. Pierce ECL Western blotting substrate (Thermo Scientific) was used to detect HRP activity from the secondary antibodies. CXCR4 (125 μg/ml), anti-CXCR4 (phospho S339) (0.5 μg/ml), goat anti-rabbit IgG-HRB (0.1 μg/ml) antibodies were acquired from Abcam (Cambridge, England). MEK 1/2, phospho-MEK 1/2 (Ser217/221), β-actin (13E5) rabbit (mAb), and anti-rabbit IgG antibodies were acquired from Cell Signaling Technology (Beverly, MA). Western blot gels were loaded with normalized amounts of protein throughout the experiments; chemiluminescence imaging was conducted with a FluorChem M imaging system (Proteinsimple) and analyzed with Image J.

*Enzyme-linked immunosorbent assay (ELISA):* Protein from 2D cell lysates and media were collected from approximately 8-11 x $10^6$ HCC cells after 4 days of incubation at 37˚C and 5% $CO_2$ in a T75 flask with full media. Protein from 3D cell lysates and media were collected from 0.5 x $10^6$ HCC cells after 1 day of incubation at 37˚C and 5% $CO_2$ from a type I rat tail collagen/Matrigel matrix. Protease inhibitors were added to HCC cell lysates and media which were finally stored at -20˚C. CXCL12 detection was accomplished by conducting a sandwich ELISA from a commercial kit (R&D Systems). CXCL12 levels were quantified using protein from 2-D and 3-D cell lysates and their respective media.

*Statistical analysis:* Statistical analyses were conducted using GraphPad Prism or MATLAB. For all results, one- or two-factor ANOVA was conducted, followed by Tukey's test or Bonferroni test for multiple comparisons if the F-test showed a statistically significant result.

<u>Specific Aim 1—Determine the mechanism of interstitial fluid flow-induced invasion of hepatocellular carcinoma cells</u>

Previously, we demonstrated that Huh7 and Hep3B HCC cells, but not HepG2 cells or primary rat hepatocytes, invade in response to physiologically relevant interstitial flow through the chemokine receptor CXCR4. The requirement for CXCR4 in Huh7 and Hep3B cells, but not HepG2 cells, is not due to levels of CXCR4, which are comparable in both 2-D and 3-D culture (Fig. 1). Incorporation of a CXCL12-neutralizing antibody into the invasion assay blocks flow-induced invasion of Huh7 cells, suggesting that CXCR4/CXCL12 binding is necessary (Fig. 2A). To further test if a gradient of CXCL12 is necessary, we exposed Huh7 cells to a high concentration (80 ng/ml) of exogenous CXCL12 to diminish the relative magnitude of any autocrine CXCL12 gradient, and we observed a significant reduction in interstitial flow-induced invasion (Fig. 2B). Differences in the responsiveness of Huh7 and Hep3B cells versus HepG2 cells to interstitial flow was not due to secretion of CXCL12, which was comparable between the three cell lines in 3-D conditions, though HepG2 cells notably secrete very little CXCL12 in 2-D conditions (Fig. 2C).

To determine what downstream signaling pathways mediate CXCR4/CXCL12-dependent invasion of Huh7 cells in response to interstitial flow, we screened a panel of pharmacological inhibitors in our 3-D invasion assay. Through our screen, we found that the MEK1/2 inhibitor U0126 significantly decreased interstitial flow-induced invasion (Fig. 3A). Exposure to interstitial flow did not alter total MEK1/2 levels in Huh7 cells (Fig. 3B) or phosphorylated MEK1/2 levels in any of the HCC cell lines (Fig. 3C). However, Huh7 and Hep3B cells showed significantly higher levels of MEK1/2 activation compared to HepG2 cells (Fig. 3C). Combined with the U0126 results, this suggests that MEK1/2 signaling may be required for interstitial flow-induced invasion.

Specific Aim 2—Elucidate the effects of an HBV infection on the response of hepatocytes to interstitial fluid flow

To determine whether HBV infection alters liver cell responses to interstitial flow, we first needed to implement an *in vitro* model of HBV infection. Since cells cannot be infected by the virus *in vitro*, we opted for delivery of HBV DNA using a plasmid vector, after determining that adenovirus (another vector option) appeared to increase invasion independent of the delivered DNA. After measuring HBV core protein levels post-transfection to determine an optimal testing window, we opted for experimentation 48 h post-transfection. Using the aforementioned 3-D invasion assay, we quantified invasion of Huh7 cells transfected with HBV DNA and showed that the introduction of pGEMHBV increased invasion in response to interstitial flow compared to untransfected cells and cells transfected with the empty pGEM plasmid (Fig. 4).

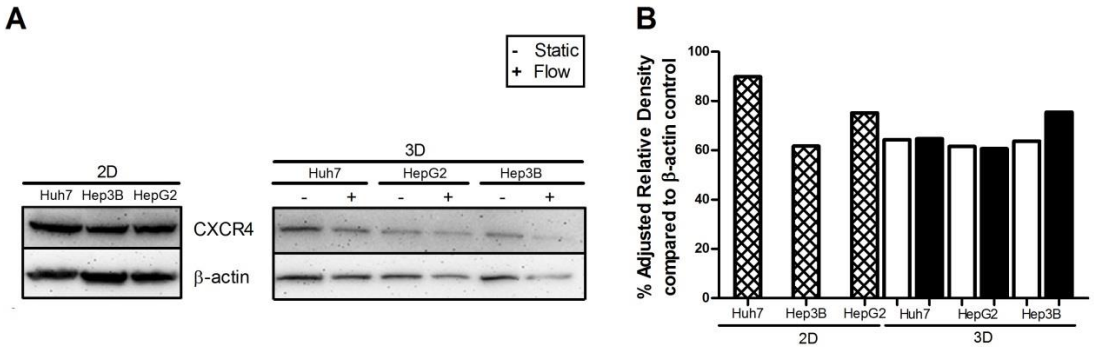


Figure 1: CXCR4 levels do not vary between HCC cell lines. (A) CXCR4 is detected in HCC cell lines in both 2D and 3D lysates. CXCR4 = 43 kDa. Static 3D sample, (-) and Flow 3D Sample, (+). (B) Quantitative western blot analysis of CXCR4. Percentage adjusted relative density compared to loading control of respective sample. Static 3D sample, (white bar); Flow 3D Sample, (black bar)

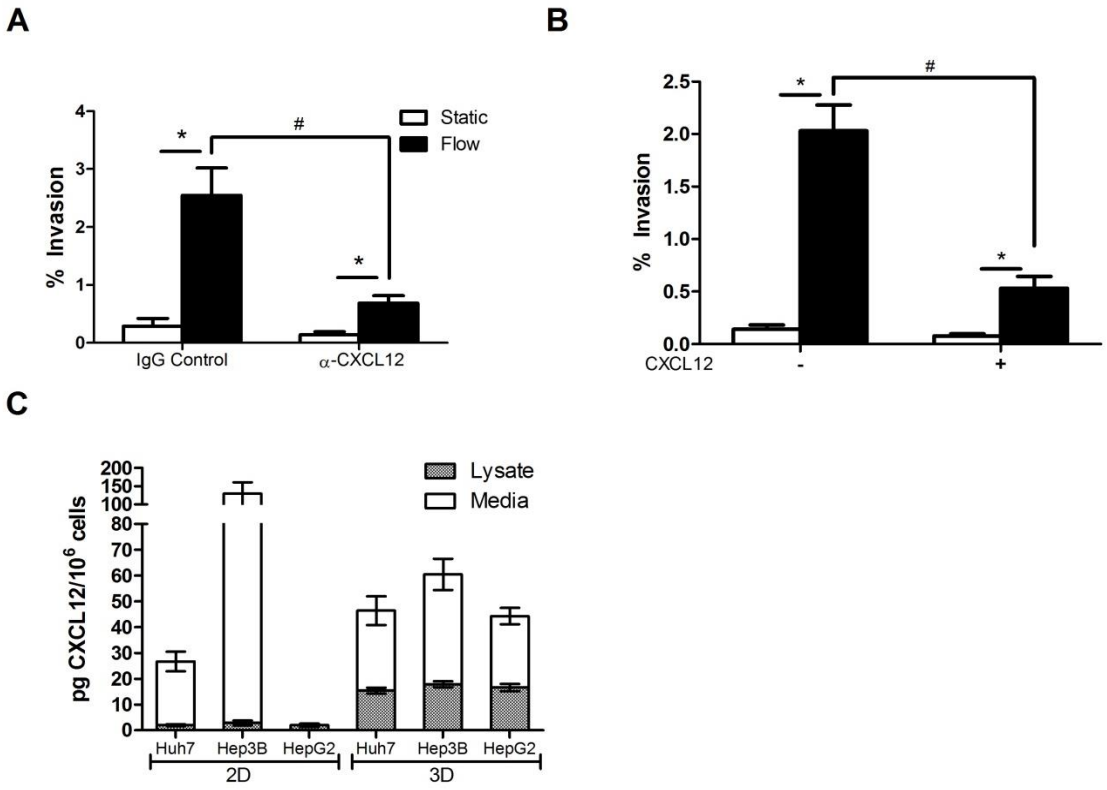


Figure 2: A CXCL12 gradient is necessary for interstitial flow-induced invasion of Huh7 cells. (A) Huh7 cells treated with CXCL12 neutralizing antibody and an isotype control (3 µg/ml) for 24 hours in a 3-D invasion assay (n = 9). * $p < 0.05$ between each respective treatment condition. # $p < 0.05$ between static vs. flow conditions of the two treatment options. (B) Invasion assay (n=12) on Huh7 cells with/without exogenous CXCL12 (80 ng/ml) media was conducted to observe changes in flow-induced cellular invasion. Test condition: + = exogenous CXCL12 added to media; - no exogenous CXCL12 present in media. * $p < 0.05$; # $p < 0.05$. (C) Average CXCL12 levels in 2-D and 3-D lysates (static) and respective media was measured with ELISA.

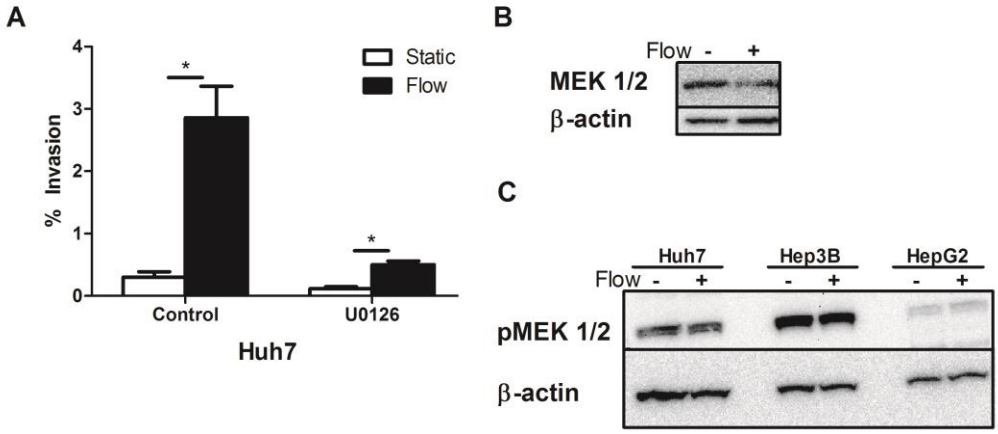


Figure 3: Flow-induced HCC cell invasion is mediated by the MEK 1/2 pathway. (A) MEK 1/2 inhibitor (U0126) at 25 μM incorporated in the 3D invasion assay with Huh7 cells (n = 5). * $p < 0.05$. (B) Western blot conducted to detect the presence of MEK 1/2 from protein collected from Huh7 cells under static and flow. (C) Phosphorylated MEK ½ (pMEK1/2) protein levels in Huh7, Hep3B, and HepG2 cells under static and interstitial flow conditions.

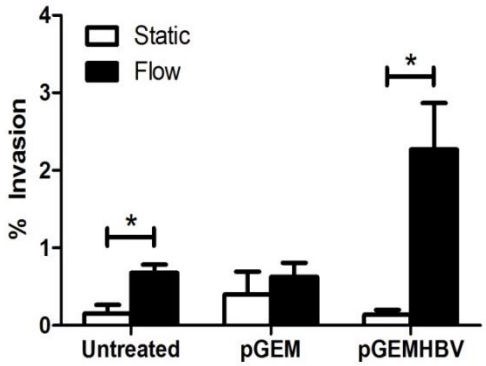


Figure 4: Interstitial flow-induced invasion of Huh7 cells is enhanced by HBV. Huh7 cells transfected with a plasmid containing HBV DNA showed a significantly stronger response to interstitial flow than normal Huh7 cells or cells transfected with the empty pGEM plasmid. * $p < 0.05$. Sample size n = 3 for all conditions.

## Research Project 10: Project Title and Purpose

*Encapsulation Systems with Tunable Permeability for Improved Stability and Release Profile of Encapsulated Materials of Biomedical Importance* – Oxidation of encapsulated bioactive molecules such as drugs and vitamins results in loss of their activity. The oxidation process within these encapsulation systems is initiated by transport of oxidants such as free radicals generated in the aqueous phase and transported across the interfacial layer of the encapsulation system and into the encapsulation system**.** In the present research, we propose to design

encapsulation systems with tunable permeability to minimize the transport of these free radicals across encapsulation system, thus reducing the oxidation of encapsulated materials of biomedical importance. Tunable permeability will also enable enhanced control over the release profile of these encapsulated bioactive molecules.

**Duration of Project**

1/1/2012 – 6/30/2013

**Summary of Research Completed**

This project ended during a prior state fiscal year. For additional information, please refer to the Commonwealth Universal Research Enhancement C.U.R.E. Annual Reports on the Department's Tobacco Settlement/Act 77 web page at http://www.health.state.pa.us/cure.